Structural Engineering and Mechanics, *Vol. 75, No. 1 (2020) 101-108*
DOI: https://doi.org/10.12989/sem.2020.75.1.101

Anisotropic continuum damage analysis of thin-walled pressure vessels under cyclic thermo-mechanical loading

Azam Surmiri[1], Ali Nayebi*[1], Hojjatollah Rokhgireh[2] and Ahmad Varvani-Farahani[3]

[1]*Mechanical Engineering Department, Shiraz University, Shiraz, Iran*
[2]*Mechanical Engineering Department, University of Larestan, Lar, Iran*
[3]*Department of Mechanical and Industrial Engineering, Ryerson University, Toronto, Canada*

(Received November 13, 2019, Revised February 11, 2020, Accepted February 12, 2020)

Abstract. The present study intends to analyze damage in thin-walled steel cylinders undergoing constant internal pressure and thermal cycles through use of anisotropic continuum damage mechanics (CDM) model coupled with nonlinear kinematic hardening rule of Chaboche. Materials damage in each direction was defined based on plastic strain and its direction. Stress and strain distribution over wall-thickness was described based on the CDM model and the return mapping algorithm was employed based on the consistency condition. Plastic zone expansion across the wall thickness of cylinders was noticeably affected with change in internal pressure and temperature gradients. Expansion of plastic zone over wall-thickness at inner and outer surfaces and their boundaries demarking elastic and plastic regions was attributed to the magnitude of damage induced over thermo-mechanical cycles on the thin-walled samples tested at various pressure stresses.

Keywords: anisotropic Continuum Damage Mechanics (CDM); cyclic loading; nonlinear kinematic hardening; return mapping algorithm; cylindrical pressure vessel

1. Introduction

In design of engineering components such as pressure vessels, boilers and turbine blades undergoing severe cyclic thermo-mechanical loads, materials inelastic deformation promotes damage in different directions leading to failure. The continuum damage mechanics (CDM) theory was first introduced by Kachanov (1958) to describe how materials damage influenced mechanical properties. To simplify the CDM theory, he defined damage progress on the basis of materials isotropic response with consistent degradation of mechanical properties along different directions. Lemaitre and coworkers (Lemaitre and Desmorat 2005, Lemaitre *et al*. 2000) assessed damage initiation and growth of cylindrical pressure vessel samples undergoing monotonic loads through use of isotropic CDM theory and concluded that the theory is yet to assess damage in ductile materials with anisotropic response Nouailhas (1980) and Benzerga *et al*. (2004) performed uniaxial tests respectively on XC38 and XC52 steel samples and reported anisotropic damage response in the material. Tests performed by Tests performed by Cordebois and Sidoroff (1982) and Chow and Wang (1987) demonstrated that damage progress along loading direction was twice in magnitude as compared to that of transverse direction in Al2024 samples. Pi *et al*. (2014) developed a dynamic plasticity model to account for nonlinear elasticity, coupled with deviatoric behavior and thermo-dynamical consistence. Based on the decomposition of the stress tensor, a framework for anisotropic materials was employed. In their studies (Benzerga *et al*. 2004, Cordebois and Sidoroff 1982, Chow and Wang 1987) plastic strain was reported as the dominant parameter to induce anisotropic response in damaged samples. Over last half-century several research endeavors have been carried out to study inelastic response of cylindrical pressure vessels under thermo-mechanical cyclic loadings (Varvani-Farahani and Nayebi 2018). Since earlier model of Hill (1950) developed on the basis of isotropic hardening description back in 1950 and inclusion of plastic response and demarcation of elastic/plastic boundaries through work of Bree in 1967, research on linear and non-linear response of materials through use of kinematic hardening rules were pursued to assess materials damage under mechanical and/or thermal cyclic loading conditions (Beesley *et al*. 2017, Nayebi 2010, Nayebi 2010, Nayebi and El Abdi 2002, Sirumbal-Zapata *et al*. 2018). Surmiri *et al*. (2018) lately coupled Chaboche's nonlinear kinematic hardening rule with Lemaitre's anisotropic CDM to assess shakedown-ratcheting of Bree's problem in a thin-walled sphere undergoing cyclic thermo-mechanical loading conditions. They discussed parameters influencing nonlinear damage progress as the magnitude of pressure stress and temperature distribution over wall thickness moved elastic/plastic boundaries within an anisotropic material response.

The use of anisotropic damage theory has been a challenge to evaluate materials response of components undergoing cyclic thermo-mechanical loads due to its mathematical complexity and framework. The present study intends to attribute continuum damage to materials anisotropic response of cylindrical pressure vessel samples undergoing cyclic thermo-mechanical loading conditions.

*Corresponding author, Ph.D., Professor
E-mail: nayebi@shirazu.ac.ir

Copyright © 2020 Techno-Press, Ltd.

ISSN: 1225-4568 (Print), 1598-6217 (Online)

Cylindrical samples consisted of constant internal pressure and cyclic thermal gradient across the wall thickness. The anisotropic response was encountered into the framework on the basis of plastic strain as the prime component to assess damage over thermo-mechanical cycles of thin-walled cylinders. Incremental stress-strain relation was developed and the return mapping algorithm was used to obtain the response of the pressure vessel under cyclic loads. The magnitude and gradient of temperature influenced the induced damage over inner and outer surfaces over wall-thickness. Plastic zone evolution near the inner and outer surfaces was distinctly separated from elastic region as the magnitude of pressure stresses increased.

2. Formulation of anisotropic continuum damage and cyclic loads

2.1. Anisotropic continuum damage model

Damage progresses as materials deforms inelastically resulting in a drop in the real effective surface, $\tilde{A}$, with respect to the area of section element, A, over the formation of cracks and voids. This makes the effective stress different from Cauchy stress and is defined as:

$$\tilde{\sigma}_{ij} = \left(H_{im}\,\sigma^{D}_{mn}\,H_{nj}\right)^{D} + \frac{\sigma_H}{1-\eta\,D_H}\,\delta_{ij} \tag{1}$$

Where σ_D, σ_H, D_H and η respectively represent deviatoric stress tensor, hydrostatic stress, mean damage parameter, a constant η=3. The effective damage tensor H in Eq. 1 is defined based on damage tensor D. Lemaitre's anisotropic damage model is yielded as (Surmiri *et al*. 2018):

$$\dot{D}_{ij} = \left(\frac{Y}{S}\right)^{s}\left|\dot{\varepsilon}^{p}_{ij}\right| \tag{2}$$

where Y is the effective elastic strain energy density given by $Y = \tilde{\sigma}_{eq}R_v/(2E)$. Terms R_v and $\tilde{\sigma}_{eq}$ are respectively effective triaxiality function and equivalent effective stress and are defined as:

$$R_v = \frac{2}{3}(1+\nu) + 3(1-2\nu)\left(\frac{\tilde{\sigma}_H}{\tilde{\sigma}_{eq}}\right) \tag{3}$$

The yield surface for ductile materials is defined through the von-Mises criterion as:

$$f = (\tilde{\boldsymbol{\sigma}} - \mathbf{X})_{eq} - \sigma_y = [\frac{3}{2}(\tilde{\boldsymbol{\sigma}}^{D} - \mathbf{X}^{D}) : (\tilde{\boldsymbol{\sigma}}^{D} - \mathbf{X}^{D})]^{\frac{1}{2}} - \sigma_y \tag{4}$$

The yield surface center evolves according to the Chaboche's nonlinear kinematic hardening rule as:

$$\begin{aligned} d\boldsymbol{X} &= \sum_{m=1}^{3} d\boldsymbol{X}^{m} \\ d\boldsymbol{X}^{m} &= \frac{2}{3}C^{m}d\boldsymbol{\varepsilon}^{p} - \gamma^{m}\,\boldsymbol{X}^{m}d\varepsilon^{p}_{eq} \end{aligned} \tag{5}$$

The flow rule is expressed as:

$$d\boldsymbol{\varepsilon}^{p} = d\lambda\frac{\partial f}{\partial \boldsymbol{\sigma}} = d\lambda\boldsymbol{n} \tag{6}$$

where $d\lambda$ is plastic multiplier and $\boldsymbol{n}$ is normal vector to the yield surface. The plastic strain rate is defined as:

$$\begin{aligned} \dot{\boldsymbol{\varepsilon}}^{p} &= \left[\boldsymbol{H}\,\dot{\boldsymbol{e}}^{\boldsymbol{p}}\,\boldsymbol{H}\right]^{D} \\ d\boldsymbol{e}^{\boldsymbol{p}} &= \frac{3}{2}\frac{\tilde{\boldsymbol{\sigma}}^{D} - \boldsymbol{X}^{D}}{\left(\tilde{\boldsymbol{\sigma}}^{D} - \boldsymbol{X}^{D}\right)_{eq}}d\lambda \end{aligned} \tag{7}$$

and the normal vector $\boldsymbol{n}$ is defined as:

$$\boldsymbol{n} = \left[\frac{3}{2}\boldsymbol{H}\frac{\tilde{\boldsymbol{\sigma}} - \boldsymbol{X}}{\left(\tilde{\boldsymbol{\sigma}} - \boldsymbol{X}\right)_{eq}}\boldsymbol{H}\right]^{D} \tag{8}$$

To determine plastic coefficients, the consistency condition should be satisfied as:

$$df = 2\left(\tilde{\boldsymbol{\sigma}}^{D} - \mathbf{X}^{D}\right)\left(d\,\tilde{\boldsymbol{\sigma}}^{D} - d\,\mathbf{X}^{D}\right) = 0 \tag{9}$$

Through substituting terms $d\tilde{\sigma}^{D}$ and $d\boldsymbol{X}^{D}$ respectively from Eq. 1 and Eq. 5 into Eq. 9, the consistency condition is developed as:

$$df = 2\left(\tilde{\boldsymbol{\sigma}}^{D} - \mathbf{X}^{D}\right)\left\{\begin{aligned} &\left[\mathbf{H}\mathbf{H} - \frac{1}{3}\mathbf{H}\mathbf{H}\mathbf{I}\right]d\,\tilde{\boldsymbol{\sigma}}^{D} + \left(\mathbf{A}^{-1} : \left(\mathbf{H}^{2}\underline{\otimes}\mathbf{H}^{2}\right) : d\,\mathbf{D}\right)\times \\ &\left[\mathbf{I}\underline{\otimes}\left(\mathbf{H}\boldsymbol{\sigma}^{D}\right) + \left(\mathbf{H}\boldsymbol{\sigma}^{D}\right)\underline{\otimes}\mathbf{I} - \frac{1}{3}\mathbf{I}\left(\begin{matrix}\boldsymbol{\sigma}^{D}\mathbf{H} \\ +\mathbf{H}\boldsymbol{\sigma}^{D}\end{matrix}\right)\right] \\ &- d\,\mathbf{X}^{D} \end{aligned}\right\} = 0 \tag{10}$$

In Eq. 10, $\boldsymbol{A}$ is defined as:

$$\boldsymbol{A} = \boldsymbol{H}\underline{\otimes}\boldsymbol{I} + \boldsymbol{I}\underline{\otimes}\boldsymbol{H} \tag{11}$$

The special tensor product $\boldsymbol{A}\underline{\otimes}\boldsymbol{B}$ is presented as:

$$(A\underline{\otimes}B)_{ijkl} = A_{ik}B_{jl} \tag{12}$$

If $d\boldsymbol{X}^{D} = \mathbf{A}'d\lambda$ and $d\mathbf{D} = (\bar{Y}/S)^{s}|\mathbf{n}|d\lambda = \mathbf{B}d\lambda$, the plastic multiplier is obtained as:

$$d\lambda = \frac{\left(\tilde{\boldsymbol{\sigma}}^{D} - \mathbf{X}^{D}\right)\left(\mathbf{H}\underline{\otimes}\mathbf{H} - \frac{1}{3}\mathbf{H}\mathbf{H}\otimes\mathbf{I}\right)d\boldsymbol{\sigma}^{D}}{\left[\begin{aligned} &\left(\tilde{\boldsymbol{\sigma}}^{D} - \mathbf{X}^{D}\right)\mathbf{A}' - \left(\tilde{\boldsymbol{\sigma}}^{D} - \mathbf{X}^{D}\right)\times \\ &\left\{\mathbf{I}\underline{\otimes}\left(\mathbf{H}\boldsymbol{\sigma}^{D}\right) + \left(\mathbf{H}\boldsymbol{\sigma}^{D}\right)\underline{\otimes}\mathbf{I} - \frac{1}{3}\mathbf{I}\left(\boldsymbol{\sigma}^{D}\mathbf{H} + \mathbf{H}\boldsymbol{\sigma}^{D}\right)\right\}\times \\ &\left(\mathbf{A}^{-1} : \left(\mathbf{H}^{2}\underline{\otimes}\mathbf{H}^{2}\right) : \mathbf{B}\right) \end{aligned}\right]} \tag{13}$$

Developed Eqs. (1-13) are employed to assess anisotropic damage response in thin-walled pressure vessels under cyclic thermo-mechanical loading conditions.

2.2 Cylindrical pressure vessel modeling

Thin-walled cylindrical pressure vessel samples were tested under constant internal pressure and cyclic

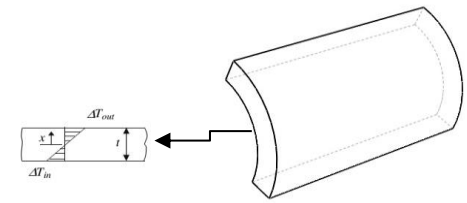

(a)

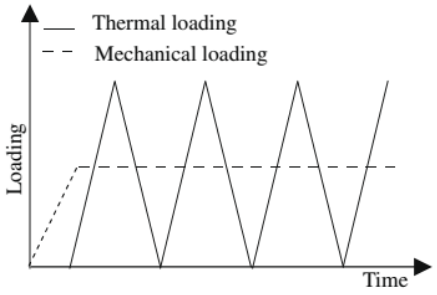

(b)

Fig. 1 a) Geometry and the temperature gradient across the wall thickness of a thin cylinder and (b) constant internal pressure and cyclic loads

temperature gradient across the thickness (Shahani and Momeni Bashusqeh 2012) to construct Bree diagram (Bree 1967). The radius and wall thickness of hollow cylinder are r and t, respectively. The temperature variation in the wall thickness was assumed linear as shown in Fig. 1**.**

The equilibrium of forces in cylinder leaded to set Eq. (14) as:

$$\int_{-t/2}^{t/2}\sigma_\theta dx = pr$$
$$\int_{-t/2}^{t/2}\sigma_z dx = \frac{pr}{2} \tag{14}$$

Based on the Hooke's law, the total strain is defined through summation of ε^e, elastic strain, ε^T, thermal strain and ε^p and plastic strains as:

$$\boldsymbol{\varepsilon} = \frac{1}{E}\tilde{\boldsymbol{\sigma}} - \frac{\upsilon}{E}\left[tr(\tilde{\boldsymbol{\sigma}})\mathbf{I} - \boldsymbol{\sigma}\right] + \alpha\Delta T\mathbf{I} + \boldsymbol{\varepsilon}^p \tag{15}$$

where $\tilde{\sigma}_r$, $\tilde{\sigma}_\theta$ and $\tilde{\sigma}_z$ are the effective radial, hoop and axial stresses in the cylindrical pressure vessel. Effective stresses in terms of strains can be determined through Eq. (14). Both hoop and axial strains across the wall thickness are taken constant (Bree 1967), but the radial strain varies across the wall thickness. For given radial strain ε_r=$K_1(z)$, hoop strain ε_θ=K_2 and axial strain ε_z=K_3, effective stress is expressed in general as:

$$\tilde{\boldsymbol{\sigma}} = \frac{E}{(1+\nu)(2\nu-1)}\begin{bmatrix}\alpha\Delta T(1+\nu)\boldsymbol{I} + \nu(2\boldsymbol{\varepsilon} - \varepsilon_{kk}\boldsymbol{I}) + \\ (1-2\nu)\boldsymbol{\varepsilon}^p - \boldsymbol{\varepsilon}\end{bmatrix} \tag{16}$$

Small value of radial stress is neglected, reducing the state of stress to plane stress condition. Radial stress component is expanded based on Eq. (1) as:

$$\sigma_r = (1-D_r)\tilde{\sigma}_r - (1-D_r)\times \left[\frac{(1-D_r)\tilde{\sigma}_r + (1-D_\theta)\tilde{\sigma}_\theta + (1-D_z)\tilde{\sigma}_z}{3(1-D_H)}\right] + (1-\eta D_H)\left(\frac{\tilde{\sigma}_r + \tilde{\sigma}_\theta + \tilde{\sigma}_z}{3}\right) \tag{17}$$

The hoop stress and axial stress components are expanded in a similar manner. Eq. 18 shows the other components of stress tensor.

$$\sigma_\theta = (1-D_\theta)\tilde{\sigma}_\theta - (1-D_\theta)\times \left[\frac{(1-D_r)\tilde{\sigma}_r + (1-D_\theta)\tilde{\sigma}_\theta + (1-D_z)\tilde{\sigma}_z}{3(1-D_H)}\right] + (1-\eta D_H)\left(\frac{\tilde{\sigma}_r + \tilde{\sigma}_\theta + \tilde{\sigma}_z}{3}\right)$$
$$\sigma_z = (1-D_z)\tilde{\sigma}_z - (1-D_z)\times \left[\frac{(1-D_r)\tilde{\sigma}_r + (1-D_\theta)\tilde{\sigma}_\theta + (1-D_z)\tilde{\sigma}_z}{3(1-D_H)}\right] + (1-\eta D_H)\left(\frac{\tilde{\sigma}_r + \tilde{\sigma}_\theta + \tilde{\sigma}_z}{3}\right) \tag{18}$$

To further express stress components in Eq. (17) and Eq. (18) as function of strain components in different directions, effective stresses from Eq. (16) are substituted into Eq. (17) and Eq. (18). In the thin-walled cylinders, the radial stress is neglected and the radial strain is expressed in terms of hoop and axial strain components. Axial and hoop strain components are then determined through equilibrium Eq. (14) and Eq. (17) to relate stress and strain components. Increment of plastic strain tensor is obtained through Eq. (7). For axisymmetric loading and problem geometry, Eq. (7) is rewritten as:

$$d\boldsymbol{\varepsilon}^p = \frac{3}{2}d\lambda(\tilde{\boldsymbol{\sigma}} - \mathbf{X})_{eq}\begin{bmatrix}\frac{\tilde{\sigma}_r^D - X_r}{1-D_r} & 0 & 0 \\ 0 & \frac{\tilde{\sigma}_\theta^D - X_\theta}{1-D_\theta} & 0 \\ 0 & 0 & \frac{\tilde{\sigma}_z^D - X_z}{1-D_z}\end{bmatrix}^D \tag{19}$$

2.3 Numerical relations based on the return mapping algorithm

The framework was developed on the basis of anisotropic continuum mechanics and the Chaboche kinematic hardening rule to assess nonlinear damage in steel samples. Return Mapping Algorithm (RAM) was employed to numerically solve damage problem. Increments of stress-strain and their hysteresis loops were formulated based on the anisotropic continuum damage model of Lemaitre and the return mapping algorithm was utilized to achieve consistency condition. The algorithm

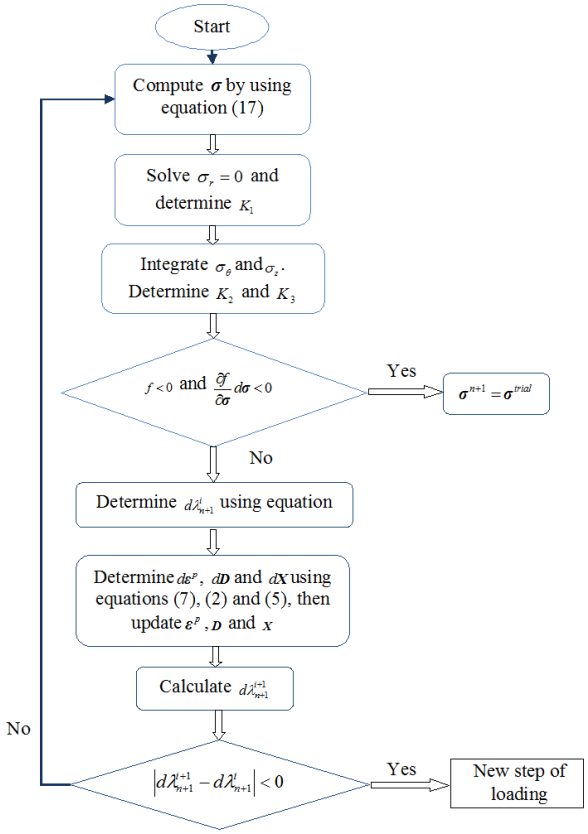

Fig. 2 Numerical algorithm and flowchart developed based on the return mapping algorithm

consisted of two steps (i) elastic prediction and (ii) plastic correction. Loads were applied in small increments. Stress increments were determined through trail procedure assuming that plastic strain increment and related damage parameter stayed consistent. Onset of yielding in each layer of the thin-walled cylinder was continuously monitored to determine plastic multiplier increment. Solution procedure was then carried out by Kuhn-Tucker condition (Simo and Hughes 2006). The trial parameters were updated based on the plastic multiplier solution. The plastic multiplier increment was obtained by the consistency condition given in equation (8). The developed numerical algorithm and its flowchart are presented in Fig. 2.

3. Results and discussions

3.1 Material properties

To model the cyclic response of thin-walled steel cylinders, the Chaboche nonlinear kinematic hardening model is coupled to the anisotropic continuum damage model of Lemaitre. Materials properties, Chaboche and Lemaitre coefficients (Surmiri *et al*. 2018) are given in Table 1.

Thin-walled steel cylinders are subjected to a constant internal pressure and cyclic temperature gradient to develop

Table 1 Constants for the Chaboche kinematic hardening rule and Lemaitre's anisotropic continuum damage

Young's modulus E (GPa)	200	γ_2	1
Yield Strength (MPa)	85	S	0.6
Chaboche's Constant C_1	44.14	s	1
Chaboche's Constant C_2	31.6	η	3
Chaboche's Constant C_3	1.9	Poisson's ratio υ	0.3
γ_1	616	$\alpha(10^{-6})/°C$	13
γ_2	20		

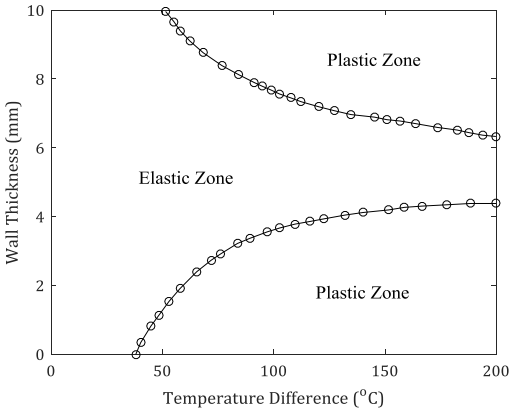

(a)

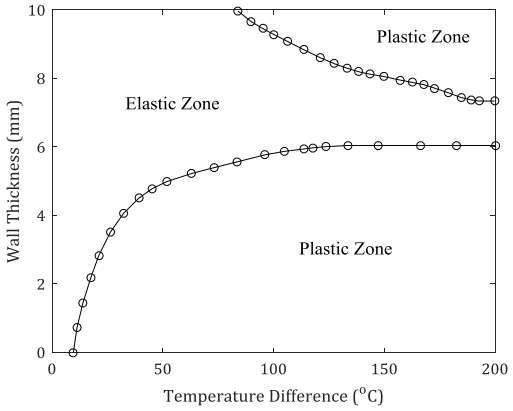

(b)

Fig. 3 a) Growth of plastic zone in the inner and outer radius versus temperature difference at σ_p=0.2. b) Growth of plastic zone in the inner and outer radius versus temperature difference at σ_p=0.8

3.2 Stress-strain analysis

Bree's diagram. Cylinders were tested with a constant internal pressure between zero to a pressure at yielding. The plastic flow occurred in the inner radius and then as temperature difference increased the plastic zone expanded towards the outer radius. As ΔT increased the magnitude of plastic zone over the outer radius became more noticeable as shown in Fig. 3. The difference between the onset of yielding in the inner and outer radii depends on the magnitude of internal pressure and *ΔT*.

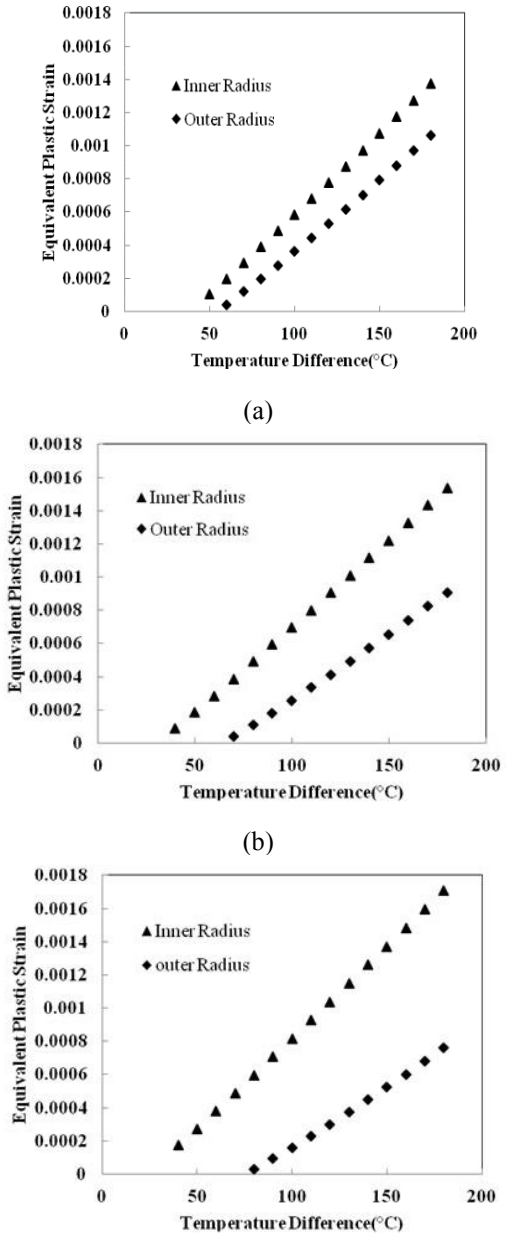

Fig. 4 Equivalent plastic strain versus temperature difference for various normalized pressure stresses (a) σ_p=0.2 (b) σ_p=0.4 and (c) σ_p=0.6

Fig. 3 shows yielding in the inner and outer surfaces at various ΔT and Δp. Plastic strain evolution over the inner and outer radii for various normalized pressure stresses $\sigma_p=pr/t\sigma_y$ of σ_p=0.2, σ_p=0.4 and σ_p=0.6 is also mapped in figure 4. Points on curves presented in Fig. 3 represent onset of yielding at any given ΔT and Δp. At the given σ_p=0.4, inner surface to yield has to experience ΔT=30°C while outer surface requires ΔT=65°C. The inner surface of cylinders experienced larger plastic deformation as compared with the outer surface at constant ΔT. As normalized pressure stress increased the difference between plastic deformation on the inner and outer surfaces became more pronounced.

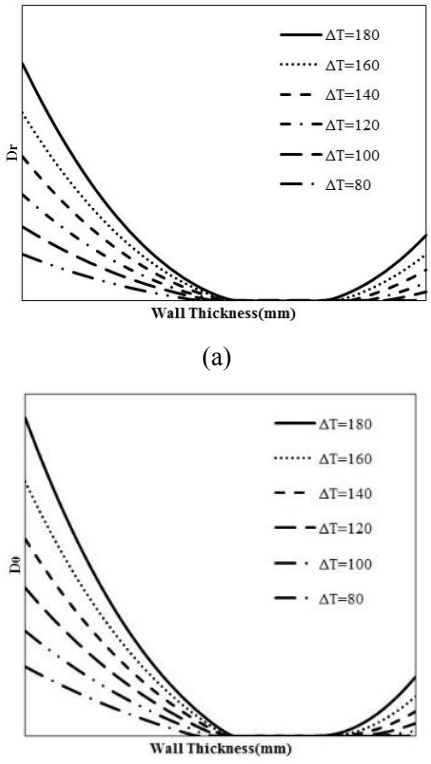

Fig. 5 Variation of (a) Dr and (b) $D\theta$ across the wall thickness for σ_p=0.6 and different temperature difference in the first cycle

Based on Lemaitre's anisotropic damage model the damage increment in each direction is proportional to the plastic strain increment in the same direction. Figure 5 presents damage variation across the wall thickness with temperature change over radial and hoop directions (D_r and D) as normalized pressure stress stayed constant σ_p=0.6. Since the plastic strain is more critical in the radial direction, damage is also more pronounced in that direction as compared with other directions. Over the first cycle, the onset of yielding occurred from the inner surface of cylindrical samples.

As stress cycles proceeded, plastic strain expanded over inner and outer surfaces as presented in Fig. 6. This figure presents evolution of the damage along hoop and radial directions for normalized pressure stresses of Δp=0.4 and 0.6 at 100th cycle.

Fig. 7 shows the variation of D_r over the wall thickness for σ_p=0.4 at ΔT=120°C at cycles 10, 20, 50 and 100. As the number of cycles in this figure increases the magnitude of damage along radial direction increased from 10th cycle to 100th cycle as high as ten times. In Figs. 6-8, the middle of wall-thickness showed no-damage zone where elastic deformation was dominant.

The magnitude of applied stress cycles noticeably influenced elastic, elastic shakedown, plastic shakedown and ratcheting zones in Bree diagram. The boundaries demarking these zones highly depended on material, rate and type of loading (Varvani-Farahani and Nayebi 2018).

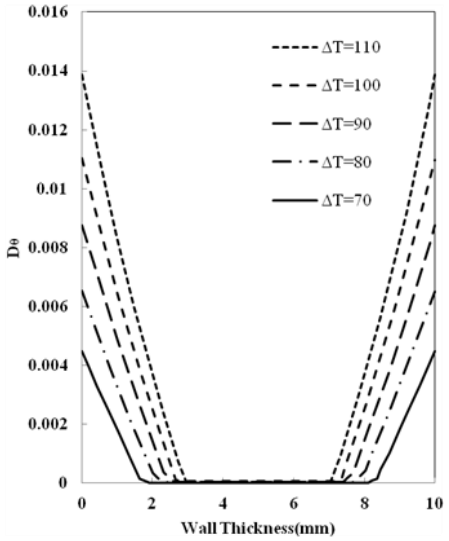

(a)

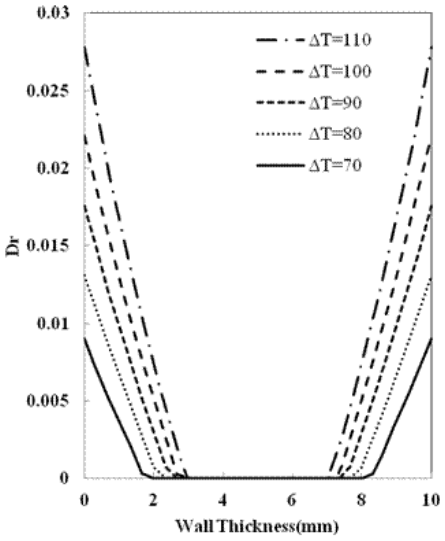

(b)

Fig. 6 Damage along hoop and radial directions after 100 cycles across the wall thickness for σ_p=0.6 (a) D_θ and (b) D_r.

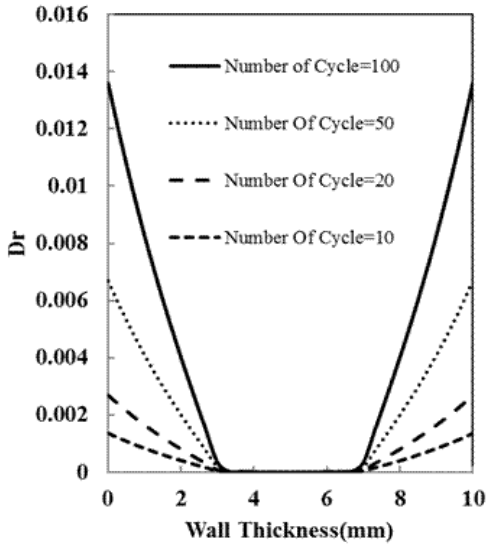

Fig. 7 Damage along radial direction Dr versus wall thickness for various cycles at given σ_p=0.4 and ΔT=120°C

Damage and its progress was described as a function of plastic strain over stress cycles enabling to assess ratcheting. For normalized pressure σ_p=0.3 and temperature difference ΔT=80°C, Fig. 8a represents stress-strain hysteresis loops over loading cycles. The progressive hoop (tangential) plastic strain over hysteresis loops represents ratcheting along this direction. **Fig. 8b** presents ratcheting curve as plastic strain accumulated over stress cycles.

Fig. 9 presents concurrent ratcheting and stress relaxation for thin-walled cylinder tested under σ_p=0. and ΔT=120°C. Stress-strain hysteresis loops are formed and mean stress relaxation occurred as a result of combined stress- and strain-controlled conditions. An increase in constant pressure and cyclic stress level led to an increase in plastic strain increment over each cycle resulting in less number of cycles to failure.

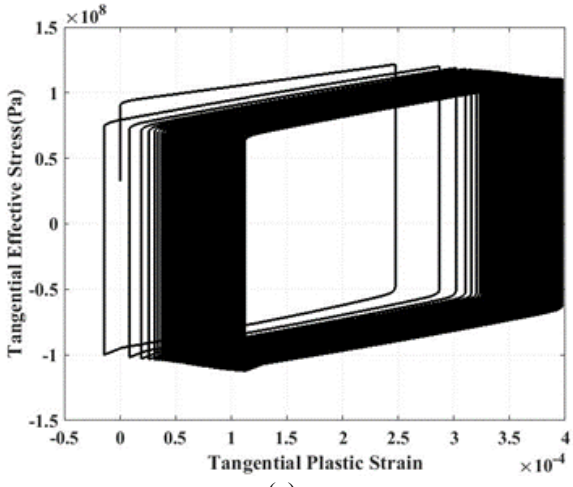

(a)

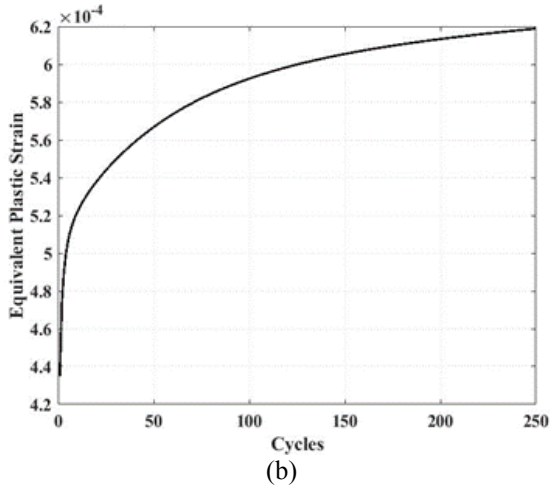

(b)

Fig. 8 Thin-walled cylinder subjected to σ_p=0.3 and ΔT=80°C (a) hysteresis loops and progressive plastic strain along tangential direction and (b) plastic strain accumulation versus number of stress cycles

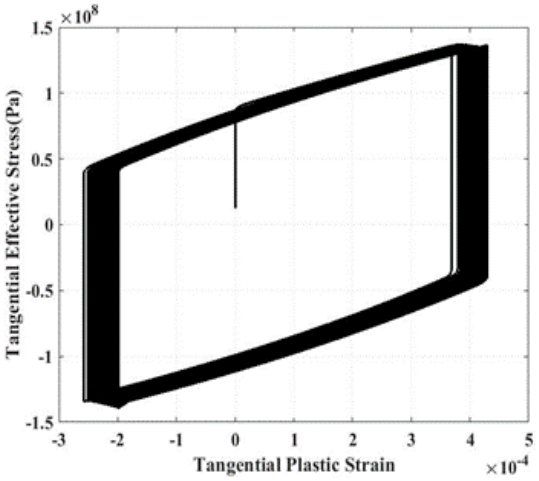

(a)

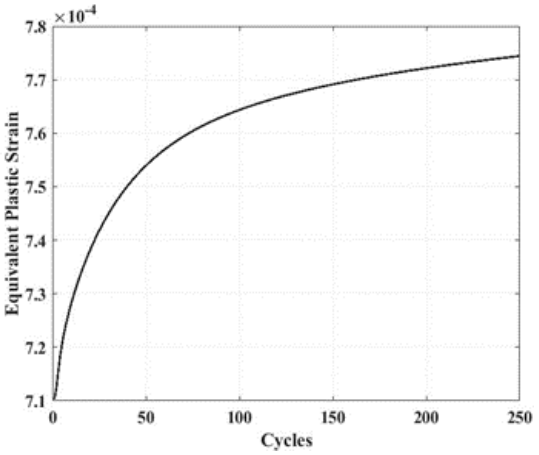

(b)

Fig. 9 Thin-walled cylinder subjected to s_p=0.3 and DT=120°C (a) hysteresis loops and progressive plastic strain along tangential direction and (b) plastic strain accumulation versus number of stress cycles

5. Conclusions

Thin-walled steel cylinders were subjected to mechanical and thermal cyclic loading conditions to evaluate damage and its influence on mechanical response of materials. Although the 4th order damage tensor definition is more accurate (Krajcinovic and Mastilovic 1995), 2nd order damage tensor was used to reduce the complexities of the equations. Anisotropic continuum damage mechanics of Lemaitre was hinged on the inelastic hardening rule of Chaboche to assess materials damage at different directions and the return mapping algorithm was used to preserve the consistency condition. The normalized internal pressure was varied from 0,2 to 0.6 and the temperature difference from 70 to 120°C. The inelastic analysis was carried out till 250 cycles to obtain the stable response. Plastic zone grew from the inner radius and expanded as thermal loads increased in magnitude. At a constant internal pressure, the outer radius of the cylinder also entered into the plastic zone over loading cycles. The growth in damage along radial direction was found larger than that along hoop direction as plastic strain was more pronounced along the radial direction. Increase of temperature difference of about 50°C, the maximum damage is approximately multiplied by 3. The plastic strain rate decreases till 150 cycles, then it becomes constant.

References

Benzerga, A. A., Besson, J. and Pineau, A. (2004), "Anisotropic ductile fracture: Part I: experiments", *Acta Materialia*, **52**(15), 4623-4638. https://doi.org/10.1016/j.actamat.2004.06.020.

Beesley, R., Chen, H. and Hughes, M. (2017), "A novel simulation for the design of a low cycle fatigue experimental testing programme", *Comput. Struct.*, **178,** 105-118. https://doi.org/10.1016/j.compstruc.2016.09.004.

Bree, J. (1967), "Elastic-plastic behaviour of thin tubes subjected to internal pressure and intermittent high-heat fluxes with application to fast-nuclear-reactor fuel elements", *J. Strain Anal.*, **2**(3), 226-238. https://doi.org/10.1243/03093247V023226.

Chow, C. L. and Wang, J. (1987), "An anisotropic theory of continuum damage mechanics for ductile fracture", *Eng. Fracture Mech.,* **27**(5), 547-558. https://doi.org/10.1016/0013-7944(87)90108-1.

Cordebois, J. and Sidoroff, F. (1982), "Anisotropic damage in elasticity and plasticity", *Journal de mecanique theorique et appliquee*, 45-60.

Hill, R. (1998), *The Mathematical Theory of Plasticity* (Vol. 11). Oxford University Press, Oxford, United Kingdom.

Kachanov, L. M. (1999), "Rupture time under creep conditions", *J. Fracture*, **97**(1-4), 11-18. https://doi.org/10.1023/A:1018671022008.

Krajcinovic, D. and Mastilovic, S. (1995), "Some fundamental issues of damage mechanics", *Mech. Mater.*, **21**(3), 217-230. https://doi.org/10.1016/0167-6636(95)00010-0.

Lemaitre, J. and Desmorat, R. (2005), *Engineering Damage Mechanics: Ductile, Creep, Fatigue And Brittle Failures*, Springer Science and Business Media, Germany.

Lemaitre, J., Desmorat, R. and Sauzay, M. (2000), "Anisotropic damage law of evolution", *Europ. J. Mech. A/Solids*, **19**(2), 187-208. https://doi.org/10.1016/S0997-7538(00)00161-3.

Nayebi, A. (2010), "Analysis of bree's cylinder with nonlinear kinematic hardening behavior", *Iran. J. Sci. Technol.*, **34**(B5), 487.

Nayebi, A. (2010), "Influence of continuum damage mechanics on the Bree's diagram of a closed end tube", *Mater. Design*, **31**(1), 296-305. https://doi.org/10.1016/j.matdes.2009.06.014.

Nayebi, A. and El Abdi, R. (2002), "Cyclic plastic and creep behaviour of pressure vessels under thermomechanical loading", *Comput. Mater. Sci.*, **25**(3), 285-296. https://doi.org/10.1016/S0927-0256(02)00218-5.

Nouailhas, D. (1980). Etude experimentale de l'endomagement de plasticite ductile anisotrope. *thčse de doctorat de l'université Paris-6*, Paris.

Pi, A., Huang, F., Wu, Y. and Zhang, Z. (2014), "Anisotropic constitutive model and numerical simulations for crystalline energetic material under shock loading", *Math. Mech. Solids*, **19**(6), 640-658. https://doi.org/10.1177/1081286513482322.

Sirumbal-Zapata, L. F., Málaga-Chuquitaype, C. and Elghazouli, A.Y. (2018), "A three-dimensional plasticity-damage constitutive model for timber under cyclic loads", *Comput. Struct.*, **195**, 47-63. https://doi.org/10.1016/j.compstruc.2017.09.010.

Surmiri, A., Nayebi, A. and Rokhgireh, H. (2018). "Shakedown-ratcheting analysis of Bree's problem by anisotropic continuum damage mechanics coupled with nonlinear kinematic hardening

model", *J. Mech. Sci.*, **137**, 295-303. https://doi.org/10.1016/j.ijmecsci.2018.01.030.
Shahani, A. R. and Momeni Bashusqeh, S. (2014). "Analytical solution of the thermoelasticity problem in a pressurized thick-walled sphere subjected to transient thermal loading", *Math. Mech. Solids*, **19**(2), 135-151. https://doi.org/10.1177/1081286512455657.
Simo, J. C. and Hughes, T. J. (2006). *Computational Inelasticity* (Vol. 7), Springer Science and Business Media, Germany.
Varvani-Farahani, A. and Nayebi, A. (2018). "Ratcheting in pressurized pipes and equipment: a review on affecting parameters, modelling, safety codes and challenges", *Fatigue Fracture Eng. Mater. Struct.*, **41**(3), 503-538. https://doi.org/10.1111/ffe.12775.

PL

Nomenclature

α	Coefficient of thermal expansion
$C_i\gamma_i$	Materials constant in Chaboche's model
ΔT	Temperature difference
η	Hydrostatic damage parameter
$d\lambda$	Plastic multiplier
σ_H	Hydrostatic stress
$\tilde{\boldsymbol{\sigma}}$	Effective stress tensor
$\boldsymbol{\sigma}^D$	Deviatoric stress tensor
σ_y	Yield stress
$\boldsymbol{D}$	Damage tensor
E	Elastic modulus
$\boldsymbol{n}$	Normal vector
p	Internal pressure
R_v	Effective triaxiality function
s	Unified damage law exponent
S	Energetic damage law parameter
$\boldsymbol{X}$	Back stress tensor
$\bar{Y}$	Effective strain energy